Int. J. Electrochem. Sci., 7 **(2012)** 10094 - 10107

International Journal of
ELECTROCHEMICAL
SCIENCE
www.electrochemsci.org

Facile Preparation of Pt/Polyallylamine/Reduced Graphene Oxide Composites and Their Application in the Electrochemical Catalysis on Methanol Oxidation

Jianguo Hu[1], *Bo He*[1], *Juan Lu*[1], *Liji Hong*[1], *Junhua Yuan*[1*,2], *Jixia Song*[3], *Li Niu*[4]

[1] College of Chemistry and Life Sciences, Zhejiang Normal University, Jinhua 321004, People's Republic of China
[2] School of Pharmacy, Hubei University of Science and Technology, Xianning 437100, People's Republic of China
[3] Jilin City Institute of Testing on Product Quality, Jilin 132013, People's Republic of China
[4] State Key Laboratory of Electroanalytical Chemistry, Changchun Institute of Applied Chemistry, the Chinese Academy of Sciences, Changchun 130022, People's Republic of China
[*]E-mail: jhyuan@zjnu.cn

Received: 27 August 2012 / *Accepted:* 17 September 2012 / *Published:* 1 October 2012

In this article, a facile synthesis of Pt/polyallylamine/reduced graphene oxide (Pt/PAA/RGO) composites is put forward by using PAA as a linker and stabilizer, which is characterized by ultraviolet visible absorption, fourier transform infrared spectroscopy, thermogravimetric analysis, X-ray Photoelectron Spectroscopy and transmission electron microscopy. In the presence of PAA, Pt nanoparticles with an average diameter of 1.4 nm are uniformly dispersed on RGO. In contrast, as to Pt/RGO prepared without PAA, Pt nanoparticles averaged 4 nm are unevenly deposited and aggregated on RGO. Pt/PAA/RGO composites exhibit a higher conversion efficiency of methanol and a faster oxidation removal of adsorbed CO during the electrochemical catalysis process due to their greater electroactive surface area. The molecular pathway of methanol oxidation at the surface of Pt catalysts is revealed in the impedance measurements. The impedance response of Pt/PAA/RGO catalysts shows a capacitive, resistive, pseudoinductive or inductive behavior depending on the applied potential.

Keywords: Graphene, Pt nanoparticles, Electrocatalytic activity, Methanol oxidation.

1. INTRODUCTION

As a clean and portable source, the direct methanol fuel cell (DMFC) has attracted considerable attention because of its simplicity, high specific energy, instantaneous recharge, long service life and environmentally-benign process [1].The DMFC relies on the oxidation of methanol on metal catalysts

layer to form CO_2 [2]. Currently, Pt is one of the most effective electrocatalysts for the DMFC due to their high catalytic activity on methanol oxidation [3]. However, there are some unavoidable obstacles to the commercialization of the DMFCs when used Pt catalysts widely, because they are expensive [4], low in kinetics of methanol oxidation and vulnerable to CO poisoning [5]. Therefore the economical and efficient use of Pt catalysts should be taken into consideration during the construction of the DMFCs. Two strategies can approach this aim. Introduction of another metal alloy [5] is a popular route. Ru is a promising promoter used extensively in Pt catalysts. Alternative method is to reduce the size of Pt nanoparticles and improve their dispersion on supports [5, 6]. It is feasible to reach for the economical and efficient use of Pt catalysts [1]. On the other hand, support itself has important influence on the catalytic efficiency of Pt catalysts [6].

Carbon materials have been investigated extensively as catalyst support materials for the DMFCs, including activated carbons [7], graphite nanofibers [6], carbon nanotubes [5, 8], and tungsten carbide [9]. These carbon materials not only significantly enhance the availability of electrochemical active surface area (ESA) of electrocatalysts for electron transfer, but also provide high mass transport of reactants to the electrocatalysts [9]. The performance of catalysts is closely associated with the sizes, shapes and distribution of the nanoparticles as well as the nature of the supporting material [5, 6, 8]. Another allotrope carbon, graphene, is composed of one-atom-thick planar sheets of sp-bonded carbon atoms that are densely packed in a honeycombed network [10]. It is a superior candidate as catalyst supports for the DMFCs due to its excellent electrical properties and high specific surface areas [11].

Graphene can be prepared by Hummer and Offemanm's method, a popular and facile approach to graphene by oxidation exfoliation of graphite in aqueous solution [12]. In this strategy, graphite can be easily exfoliated into graphene oxide (GO) layers in strong acid solution by oxidation, and then GO is readily converted into (RGO) by reduction. However, this RGO is lack of stablility and dispersion in a vast majority of solvent, although that it is functionalized with oxygen containing functional groups generated in oxidation process [13]. On the other hand, RGO functionalization resulted in hole, oxygen and carbon vacancies and defects by partial oxidation of graphite, which supply Pt precursor with some sites to bind [14]. However, these sites are uneven and inadequate for Pt nanoparticle to deposit. Therefore, further modification of RGO is necessary to prepare Pt/RGO catalysts to load Pt nanoparticles with small size and high dispersion [11, 15].

Polyallylamine (PAA), a polymer containing a number of reactive amine groups, can be applied in the preparation of noble metal nanoparticle as a reducing and stabilizing agent [16, 17]. Besides, PAA can be used for further modification of RGO by chemical bonding and electrostatic adsorption [18, 19]. These unique properties make it available for the preparation Pt/RGO catalysts. However, no works have been reported on the synthesis of Pt/RGO catalysts with PAA to date. In this study, we describe a facile approach for the synthesis of Pt/PAA/RGO composites by using PAA as a linker to bind Pt nanoparticles with RGO. In addition, PAA can stabilize Pt nanoparticles to protect from aggregation. Therefore, Pt nanoparticles can be well-dispersed on the surface of granphene with small size in the presence of PAA. It can be expected that Pt/PAA/RGO composites exhibit an enhanced catalytic activity toward electrooxidation of methanol as compared to Pt/RGO without PAA.

2. EXPERIMENTAL SECTION

2.1. Reagents and materials

Graphite powders (320 meshes) were spectrum pure. Polyallylamine (20 wt% solution in water, Mw *ca.*65,000) was purchased from Aldrich. Other chemicals was analytic pure, obtained from Beijing Chemicals, China. Water was purified by a Milli-Q system.

2.2. Synthesis of GO

GO was prepared by oxidizing natural graphite powder based on a modified Hummers method as originally presented by Kovtyukhova et al [20]. The graphite powder (10 g) was put into concentrated H_2SO_4 solution (15 mL) containing $K_2S_2O_8$ (5 g), and P_2O_5 (5 g). The mixture was kept at 80 °C for 4.5 h on a hotplate. Successively, the mixture was cooled to room temperature, diluted with deionized water and filtered. This preoxidized graphite was washed on the filter until the rinse water pH became neutral, and dried in air at ambient temperature. The oxidized graphite powder (10 g) was put into cold (0 °C) concentrated H_2SO_4 (230 mL). Then, $KMnO_4$ (30 g) was added gradually under stirring and the temperature of the mixture was kept to be below 20 °C by cooling. The mixture was then stirred at 35 °C for 2 h, and distilled with deionized water (460 mL). The temperature of the mixture was increased to 98 °C and maintained for 15 min. The reaction was terminated by the addition of a large amount of deionized water (1.4 L) and 30% H_2O_2 solution (25 mL). This mixture was filtered and washed with 1:10 HCl solution (2.5 L) in order to remove metal ions. Then as-prepared GO was suspended in deionized water, and then subjected to dialysis for 3-4 days in order to completely remove metal ions and acids. Finally, the resulting purified GO powders were collected by centrifugation and air-drying.

2.3. Synthesis of Pt/PAA/RGO and Pt /RGO composites

As-prepared GO was suspended in deionized water, and subjected to dialysis for 3-4 days in order to completely remove metal ions and acids. These purified GO powders were collected by centrifugation and air-drying.

A general process for the preparation of Pt/PAA/RGO composites is described in Fig. 1: At first, 1 mL PAA dulited 20 times were dissolved in 5.0 mL GO (0.5 mg/mL) solution and ultrasonicated for 15 min. Then 0.25 mL H_2PtCl_6 aqueous solution (10 mM) was added to the resulting solution under vigorous stirring. The solution pH was adjusted to 13.0 by adding 0.4 M KOH. Subsequently, 25 mg of $NaBH_4$ solution freshly prepared was rapidly added. This mixture solution was heated at 80 ^{0}C under stirring for 1.5 h, collected after thoroughly rinsing with ethanol and deionized water, and finally vacuum-dried at room temperature for characterization. The Pt/RGO was prepared in accordance with the synthesis procedures of Pt/PAA/RGO composites without PAA.

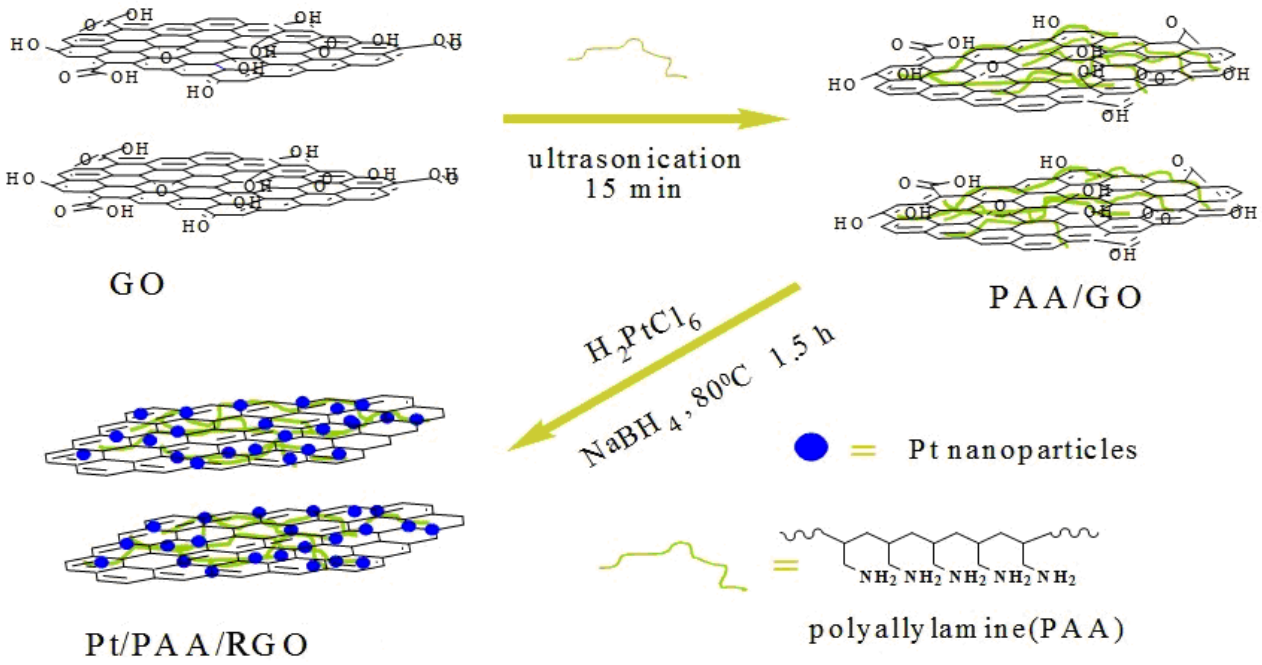

Figure 1. Illustration of the procedures to prepare Pt/PAA/RGO composites

2.4. Characterization

Ultraviolet visible absorption spectrophotometry (UV-vis) was recorded at a Hitachi U-3900 spectrometer.

Fourier Transform Infrared Spectroscopy (FT-IR) was recorded at a Bruker Vertex 70 spectrometer using KBr pellets after baseline correction.

Thermogravimetric analysis (TGA) was recorded at a Netzsch STA 449 C analyzer at a heating rate of 10 °C/min under nitrogen.

X-ray Photoelectron Spectroscopy (XPS) was recorded at an ESCALAB-MKII spectrometer with an unmonochromated Al KR X-ray source (1486.6 eV) for excitation at a base pressure of 1×10^{-10} torr. High-resolution spectra with an energy resolution of 0.85 eV were obtained at a perpendicular takeoff angle by using the pass energy of 20 and 0.05 eV steps.

Inductively coupled plasma-atom emission spectroscopy (ICP-AES) was performed on Agilent 7500ce quadrupole ICP-AES. Different catalysts, Pt/PAA/RGO and Pt/RGO, were sampled by treatment with aqua regia. RGO can not be dissolved, which can be discarded by centrifugation. Pt was dissolved and left in solution for ICP-AES analysis.

Transmission electron microscopy (TEM) images were obtained on a JEOL 2010 microscope equipped with a CCD camera by operating at 200 kV using a high-brightness LaB_6 electron gun. Samples were prepared respectively by dispersing composites in deionized water with an ultrasonic bath. A drop of 8 μL as-prepared Pt/PAA/RGO or Pt/RGO composites suspension was then gently deposited onto a carbon-coated copper grid and dried in air prior to TEM observation.

2.5 Electrochemical investigation

We used a 50 mL glass electrochemical cell comprised of three electrodes: (1) a glassy carbon disk working electrode (3 mm in diameter) embedded in Teflon, (2) a platinum wire counter electrode, and (3) a saturated calomel electrode as the reference electrode. Before use, the glassy carbon disk electrodes were carefully polished with alumina slurry. Then they were washed with deionized water, cleaned in deionized water and ethanol respectively for 20 min by ultrasonic bath.

To modify the glassy carbon disk electrode with Pt/PAA/RGO or Pt/RGO composites, 1.0 mg of as-prepared materials was dispersed in 100 μL of the deionized water. The mixture was spread and air-dried on a glassy carbon disk electrode at room temperature.

A three-electrode setup was configured with CHI 660C interfaced to a personal computer at room temperature for the electrochemical characterization of as-prepared composites (Pt/PAA/RGO or Pt/RGO) modified glassy carbon disk electrode. The electrolytic solution was bubbled with nitrogen for 15 minutes before the electrochemical experiment.

Electrochemical experiments were carried out in 0.5 M H_2SO_4 in the absence or presence of 1 M methanol. Electrochemical impedance spectroscopy (EIS) measurements were conducted without stirring. They were performed in the frequency ranged from 0.01 Hz to 100 kHz with a 5 mV of amplitude of modulation potential.

3. RESULTS AND DISCUSSION

3.1. Characterization of Pt/PAA/RGO composities

Fig.2. shows the UV absorption spectra of GO, H_2PtCl_6 and Pt/PAA/RGO aqueous solutions. The GO solution reaches peak absorption on its UV spectrum at ca. 229 nm (Fig. 2a), and H_2PtCl_6 solution alone shows its peak absorption at 258.4 nm (Fig. 2b). However, after reaction with $NaBH_4$, the peak absorption of $[PtCl_6]^{2-}$ ions disappears, suggesting the formation of Pt nanoparticles as well as the reduction of GO. Meanwhile, one of broad peak absorption occurs at 260 nm, which is attributed to the electronic conjugation within RGO (Fig. 2c) [21]. The color of the solution, which contains H_2PtCl_6, PAA and GO, changes from brown to black when $NaBH_4$ is added. The results are consistent with its variation of UV absorption before and after reduction (Fig. 2 inset).

The as-prepared graphene composites are characterized by FT-IR (Fig. 3). Fig. 3a shows the typical spectrum of GO, a broad and weak adsorption at 3229 cm^{-1} could be assigned to the O-H group, and its bending vibration O-H can be observed at 1421 cm^{-1}. The skeleton vibration of aromatic C=C occur at 1609 cm^{-1}, and the stretching vibration of carboxy C=O and ether C-O-C take place at 1734 and 1102 cm^{-1} [17], respectively. Fig. 3b shows the typical spectrum of PAA, a strong and broad adsorption located at 3424 cm^{-1} could be attributed to the N-H bond. In addition, its bending vibration is visible at 1643 cm^{-1}. The CH_2 stretching vibration is presented at 2851 and 2922 cm^{-1} [22], and its bending vibration appears at 1444 cm^{-1}. When GO is functionalized with PAA, as shown in Fig. 3c, the

typical adsorption position of PAA spectrum has remain invariant, whereas the oxygen containing groups of GO show a considerable negative shift of peak location as compared to GO.

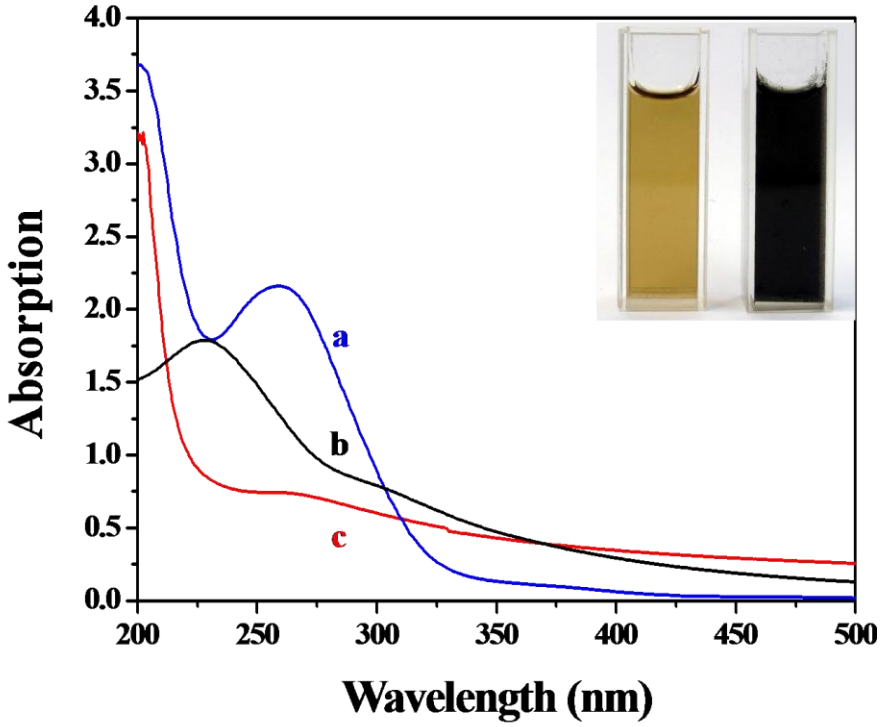

Figure 2. UV absorption spectra of H_2PtCl_6 solution (a); GO (b) and Pt/PAA/RGO (c) in water. Inset: photographs of the mixed solution of H_2PtCl_6/PAA/GO (left) and Pt/PAA/RGO (right) composites solutions.

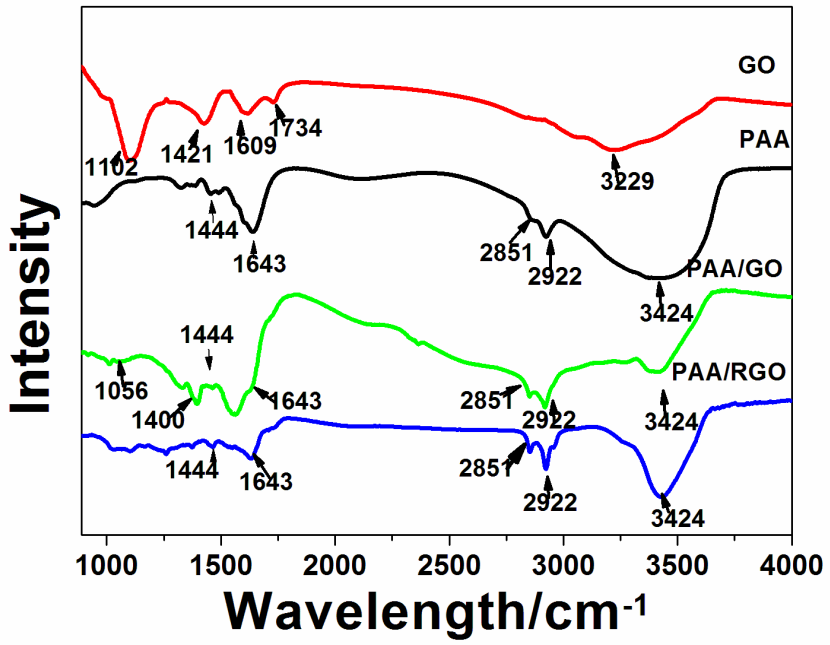

Figure 3. FT-IR spectra of GO, PAA, PAA/GO and PAA/RGO composites

For example, the positions of bending vibration O-H and stretching vibration C-O-C are decreased by 21 and 46 cm^{-1}, respectively, indicative of a strong interaction between the negative GO and positive PAA [19]. When GO reacts with $NaBH_4$, as shown in Fig. 3d, there is no observable adsorption of the oxygen containing groups from RGO, while the typical adsorption with a characteristic of PAA is still presented on the spectrum of PAA/RGO composites. The results explain that the RGO has been modified with PAA, which is in good agreement with UV observation.

The successful functionalization of RGO with PAA is also revealed in TGA curves. As shown in Fig.4, there are three mass drops in TGA curves of RGO in the temperature range from 50 to 800 ^oC, a 3.3% loss below 80 ^oC should be ascribed as the removal adsorbed water, a 5.7% loss at ca.200 ^oC should be assigned to the decomposition of the residual oxygen containing groups, and a 16.5% loss from 440 to 590 ^oC should be associated with the pyrolysis of the carbon skeleton of RGO [23]. PAA/RGO composites also shows a loss of adsorbed water by 4.4% below 80 ^oC, and two mass drops are overlapped, they can be observed in the temperature interval between 360 and 600 ^oC. The former is corresponding to decomposition of PAA, which takes place at ca. 460 ^oC, accounting for 53.1% [18]. And the latter, as discussed above, is due to graphene pyrolysis at ca. 520 ^oC, which is estimated as 11.2%.

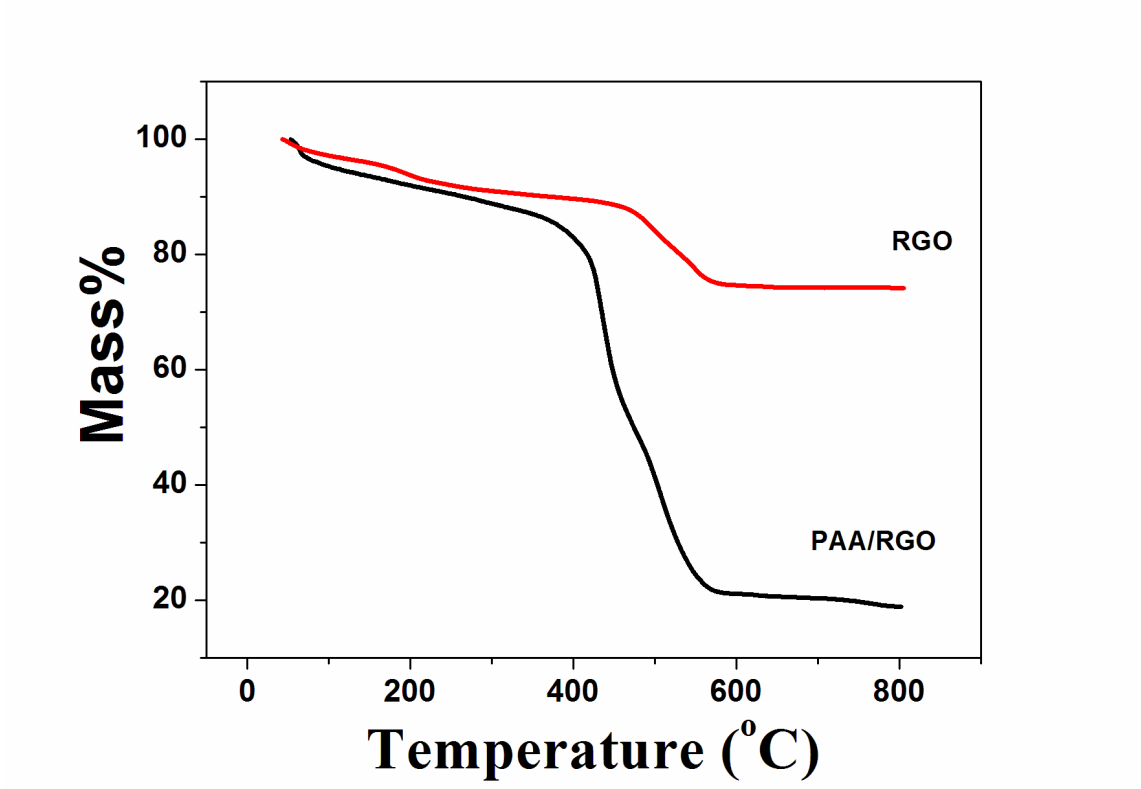

Figure 4. TGA curves of RGO and PAA/RGO composites

The XPS survey profiles of GO, PAA/RGO and Pt/PAA/RGO composites are shown in Fig.5. All of these composites had an obvious C 1s peak at 284.6 eV (carbon in C-C) and O1s peak at 531.0 eV. N 1s peaks appear at about 400 eV, which are presented at XPS curves of PAA/RGO and

Pt/PAA/RGO composite, indicating PAA is functionalized on the surface of RGO by electrostatic interaction and chemical crosslinking.

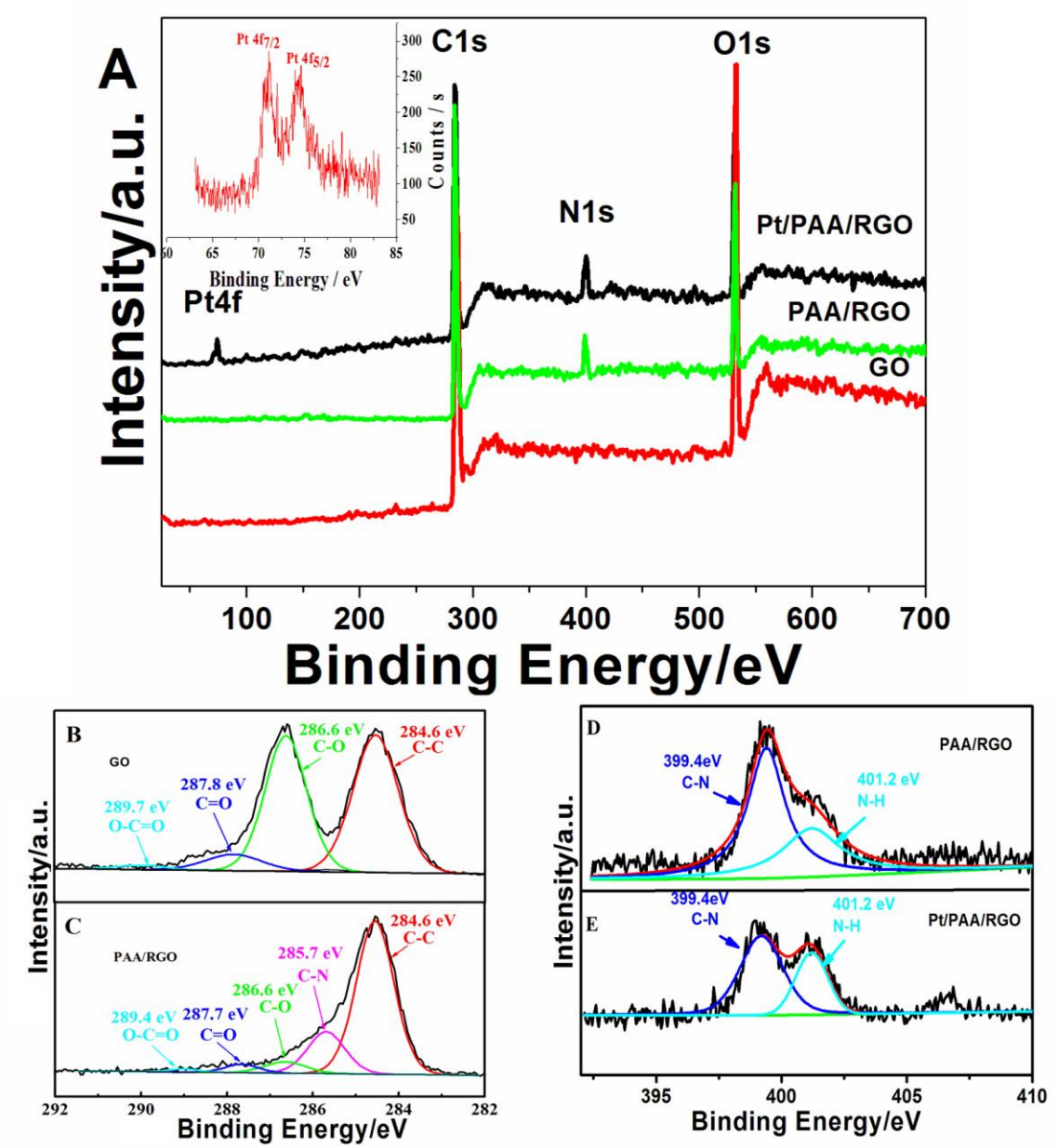

Figure 5. XPS survey profiles of GO, PAA/RGO and Pt/PAA/RGO composites (A), Insets: Pt 4f doublet; C 1s spectra of the GO (B) and PAA/RGO composites (C), and N 1s spectra of PAA/RGO (D) and Pt/PAA/RGO composites (E).

As compared to C 1s spectrum, Pt 4f XPS signal (top-right inset) is small, and unconspicuous, which can be observed on XPS curves of Pt/PAA/RGO composite. The top left inset represented the XPS signature of the Pt 4f doublet (4f 7/2 and 4f 5/2) at ca. 71.1 and 74.3 eV, which is in line with the existence of Pt nanoparticles on RGO. The C 1s XPS spectra of GO and PAA/RGO composites are shown in Fig. 5B and C, respectively. After reduction, the oxygen functional groups still exists on the

C 1s XPS spectra of PAA/RGO composites, but the absorption peaks related to the oxidized carbon species are sharply decreased, indicating that GO has been reduced in the synthesis process. In addition, there is a new peak at 285.7 eV corresponding to the existence of C-N bond, confirming the presence of PAA on PAA/RGO composites [24]. The N 1s XPS spectra of PAA/RGO and Pt/PAA/RGO composites are shown in Fig. 5D and E, respectively. The main N 1s peak at 399.4 eV is attributed to C-N groups, and a shoulder peak at 401.2 eV is associated with N-H groups [25]. As estimated by the intensity of XPS from C-N and N-H group, the molecular ratio of C-N and N-H group is 1.5 for PAA/RGO and 1 for Pt/PAA/RGO composites. The difference of N 1s XPS spectra suggests the interaction between Pt and PAA.

Fig.6. shows TEM images of Pt/RGO and Pt/PAA/RGO composites. In the absence of PAA, Pt nanoparticles are unevenly deposited and aggregated on the surface of RGO, and these aggregates are composed of several Pt nanoparticles. In the presence of PAA, Pt nanoparticles are more uniformly dispersed on the surface of RGO. Their size distributions were evaluated statistically by measuring the diameter of Pt nanoparticles on the surface of RGO in the selected area. Their average diameter is 1.4 nm, being much lower than that (4nm) of Pt nanoparticles on RGO without PAA. The results demonstrate the functionalization of RGO with PAA makes a difference in dispersion and size for the Pt nanoparticles decorated on the surface of RGO. Herein, PAA plays two important roles in the synthesis of Pt/PAA/RGO composites: a linker to supply nanoparticles with more sites to deposit and a stabilizer to protect Pt nanoparticles protect them from aggregation and overgrowth.

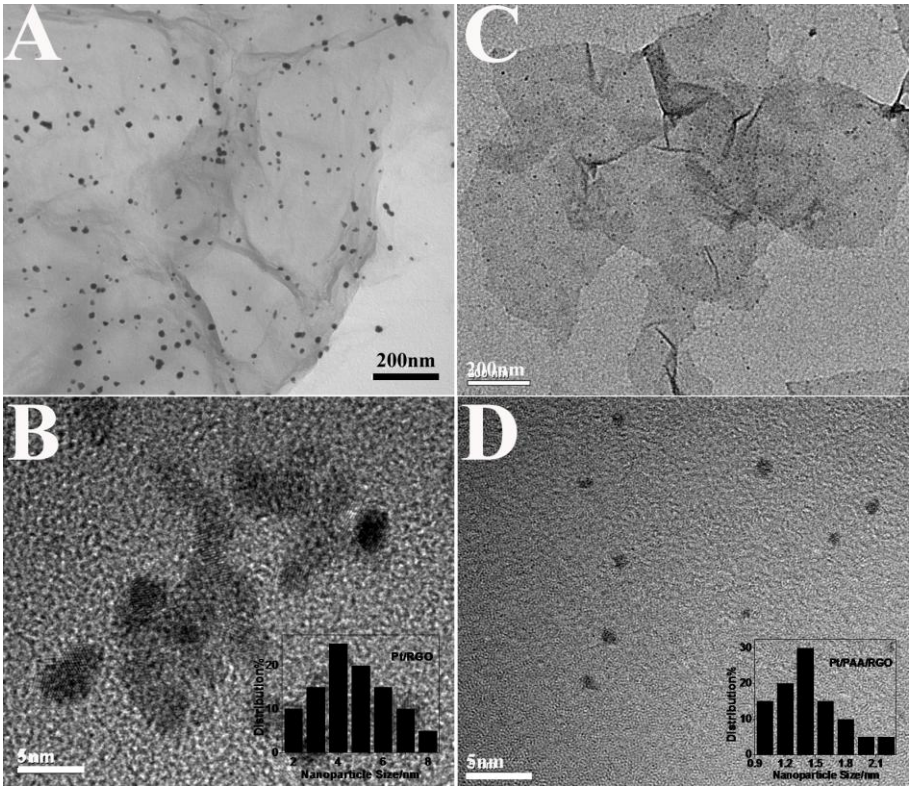

Figure 6. TEM mages of Pt/RGO (A and B) and Pt/PAA/RGO (C and D) compsites, insert: their corresponding size distributions of Pt nanoparticles on the surface of RGO

3.2. Electrochemical oxidation of methanol

The electrochemical activity of Pt/PAA/RGO catalysts is evaluated by cyclic voltammogram (CV) obtained in N_2-saturated 0.5 M H_2SO_4 solution. As shown in Fig. 7A, both the reductive adsorption region of protons in the reverse cathodic scan and the oxidative desorption region of hydrogen atom in the forward anodic scan between -0.2 and 0.1 V show signatures of polycrystalline Pt catalysts [26]. This potential region is defined as the hydrogen area, which can be used to calculate the electroactive surface area of Pt nanoparticles [8]. After the double layer charge is corrected from CV curve, ESA is determined as 22.0 $m^2 \cdot g^{-1}$ of Pt for Pt/RGO catalysts, much less than that for Pt/PAA/RGO catalysts (108.2 $m^2 \cdot g^{-1}$ of Pt). The ESA difference between Pt/RGO and Pt/PAA/RGO catalysts results from size difference of Pt nanoparticles on the surface of graphene. Expectedly, the higher ESAs of Pt/PAA/RGO catalysts should be more favorable for the electrochemical oxidation toward methanol. On the other hand, as to Pt/PAA/RGO catalysts, the oxidation of Pt surface set out from 0.605 V, and its oxidative increase up to 1.20 V. In contrast, there is no significant current response to the oxidation of Pt observed at Pt/RGO catalysts. On the other hand, an obvious reductive peak due to Pt-O species can be presented at 0.452 V for Pt/PAA/RGO catalysts, and for Pt /RGO catalysts, it takes place at 0.506 V.

Fig. 7B shows the electrochemical catalysis on methanol by Pt/PAA/RGO and Pt/RGO catalysts. The CV data are measured in N_2-saturated 0.5 M H_2SO_4 solution containing 1 M CH_3OH solution. The forward peak is due to oxidation of methanol, and the backward peak is regarded as the oxidation of adsorbed CO which results from incomplete oxidation of methanol in the forward scan [6]. During the forward potential scanning process, the peak current density (I_{MeOH}) of Pt/PAA/RGO catalysts at the potential of 0.671 V (vs. Ag/AgCl) was 310.6 $mA \cdot mg^{-1}$, nearly fivefold that of Pt/RGO catalysts (60.6 $mA \cdot mg^{-1}$). On the other hand, during the backward potential scanning process, the peak current density (I_{CO}) of Pt/PAA/RGO catalysts at the potential of 0.436 V (vs. Ag/AgCl) was 161.8 $mA \cdot mg^{-1}$, and triples that of Pt/RGO catalysts at 0.457 V (55.4 $mA \cdot mg^{-1}$). In addition, a large ratio of I_{MeOH}/I_{CO} represents a more complete methanol oxidation, less accumulation of CO-like species on the catalyst surface, and thus a better CO-tolerance [6]. I_{MeOH}/I_{CO} of Pt/PAA/RGO catalysts is 1.92, being much higher than that of Pt/ RGO catalysts (1.09). Therefore, the performance of Pt/PAA/RGO on the electrochemical oxidation of methanol can be considered superior to that of Pt/RGO catalysts.

The stability of Pt/PAA/RGO catalysts is investigated by recording the steady-state current at a fixed potential. As shown in Fig.7C, the potential of the electrode is held at 0.500 V, and the response current is monitored for a period of 3600 s. The high current observed in the initial stage originates from the double layer charging [27]. The initial current decays sharply and reaches the steady state after 500 s. In contrast, besides the current drop from capacitor that releases during the start of catalysis, a remarkable current loss can be observed on current-time (i-t) curve of Pt/RGO catalysts, which is almost extended over all the response time. The current density of Pt/PAA/RGO catalysts at the end of 3600 s is 245 $mA \cdot mg^{-1}$, 4 times higher than that of Pt/RGO catalysts (61 $mA \cdot mg^{-1}$). The stable steady state current of Pt/PAA/RGO catalysts suggests that the electrode surface undergoes less deactivation during the oxidation process [28].

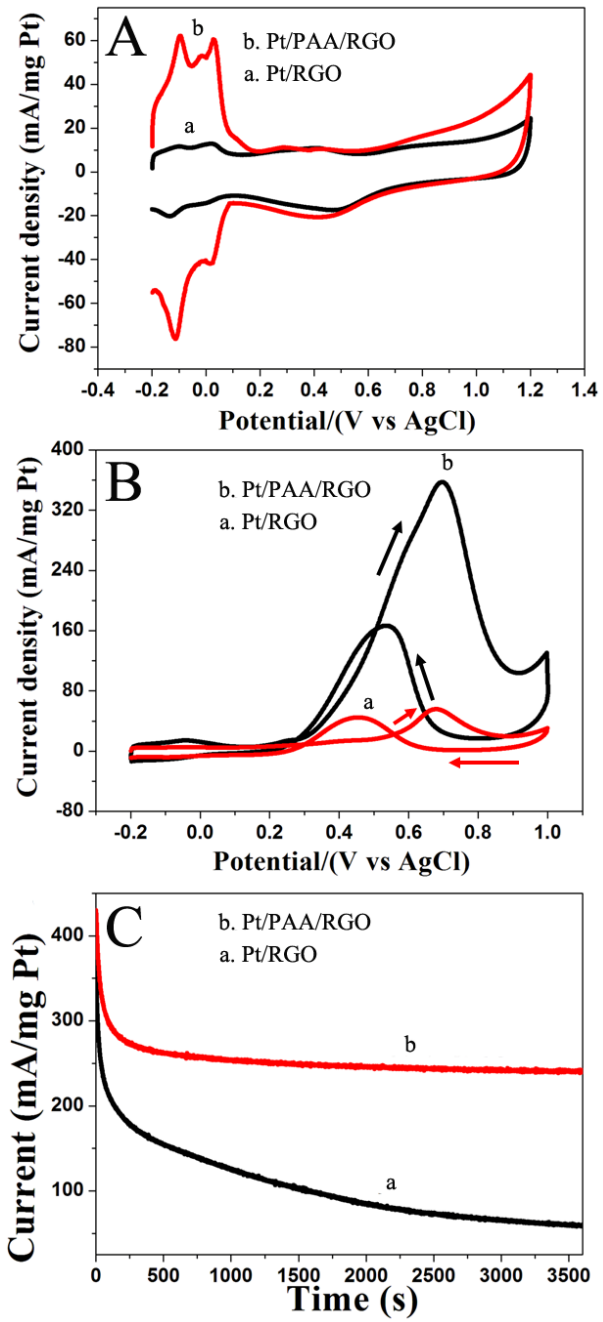

Figure 7. CVs of Pt/RGO and Pt/PAA/RGO catalysts in (A) 0.5 M N_2-saturated H_2SO_4 solution and (B) 0.5 M N_2-saturated H_2SO_4 solution containing 1 M CH_3OH, Scan rate: 0.05 Vs^{-1}. (C) I-t curves of Pt/RGO and Pt/PAA/RGO catalysts in 0.5 M N_2-saturated H_2SO_4 solution containing 1 M CH_3OH at a constant potential of 0.50 V.

Electrochemical impedance measurements are performed to investigate the electron transfer kinetics of methanol oxidation on Pt/PAA/RGO catalyst. Its impedance behavior is strongly dependent on the electrode potential. As shown in Fig. 8A, at the potentials of 0.1 and 0.2 V, Nyquist plot does not show arc, suggesting a capacitive behavior. The double layer charging and adsorption of methanol on the electrode surface influence the impedance of the electrode at these potentials. A large arc is

observed at the potential of 0.3 V, indicating the presence of resistive component. The slow electron transfer at this potential is due to the strong adsorption of poisoning intermediate CO [27]. The impedance arc decrease significantly when the applied potential is up to 0.400 V, revealing that a high electrode potential will benefit the electron transfer for methanol oxidation. On the other hand, these impedance arcs at the potential between 0.3 and 0.4 V extend to the fourth quadrant at these potentials. These impedance curves have a characteristic of the pseudoinductive behaviors, which are attributed to the oxidative removal of adsorbed CO on the nanoparticle [27]. Interestingly, at the potential of 0.5 V, a sudden change in the impedance pattern is observed. The impedance arc appears in the second quadrant at this potential.

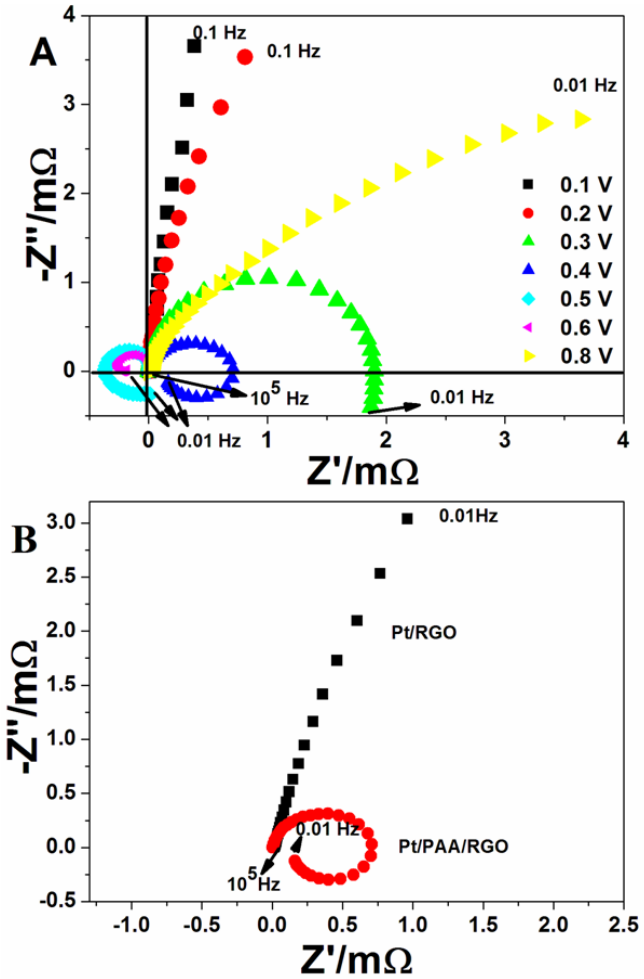

Figure 8. Impedance curves of Pt/PAA/RGO at the different potential (A), and Pt/PAA/RGO and Pt/RGO at the potential of 0.4 V (B) in 0.5 M N_2-saturated H_2SO_4 solution containing 1 M CH_3OH.

The negative Faradaic impedance suggests the existence of an inductive component, which is ascribed to the formation of chemisorbed hydroxyl species, and the chemisorbed hydroxyl species are beneficial to the oxidation of adsorbed CO [28]. At the more positive potential (0.8 V), the impedance

curves featured by a capacitive behavior appears again in the first quadrant, implying the complete removal of adsorbed CO. As discussed above, the charge transfer resistance varies with increase in the electrode potential. It decreases up to the oxidation peak potential of methanol oxidation from 0.3 to 0.6 V, and further increase (0.8 V) in the electrode potential leads to slight increase in the charge transfer resistance. It is noteworthy that the impedance behavior of Pt/RGO catalysts is different from that of Pt/PAA/RGO at the potential of 0.4 V. As shown in Fig. 8B, it is presented as a capacitive and resistive curve rather than an inductive or pseudoinductive behavior. The results strongly suggest that the structure and shape of Pt catalysts play key roles in the electrochemical activity of Pt nanoparticles. The Pt nanoparticles with a smaller size and a higher dispersion on RGO exhibit a high catalytic efficiency toward methanol oxidation, because the surface of these Pt nanoparticles are opt to be oxidized to form chemisorbed hydroxyl species at a high potential, and the latter is available to diminish CO adsorption through a oxidation reaction between CO and hydroxyl species on the surface of Pt nanoparticles.

4. CONCLUSION

We demonstrate the use of PAA as an effective linker and stabilizer for the synthesis of Pt/PAA/RGO catalysts. The Pt nanoparticles are well distributed on the surface of RGO with an average diameter of 1.4 nm. As compared to Pt/RGO composites, the as-prepared Pt/PAA/RGO catalysts show a greater electroactive surface area due to their smaller size and higher dispersion of Pt nanoparticles on RGO. In addition, Pt/PAA/RGO catalysts are higher active in the electrochemical catalysis of methanol oxidation. Their peak current density is 310.6 $mA \cdot mg^{-1}$, nearly quadrupling that at Pt/RGO catalysts. Moreover, Pt/PAA/RGO catalysts are more tolerant of CO poisoning. Their peak current ratio between the oxidation of methanol and adsorbed CO is 1.92, being higher than that of Pt/RGO catalysts (1.09). Impedance measurements indicate the formation of different reaction intermediates during the methanol oxidation process. The transition of capacitive to resistive at the lower potentials and resistive to pseudoinductive and then to inductive behaviors at high potentials have been observed at Pt/PAA/RGO catalysts. The electron transfer kinetics for the oxidation of methanol is fast at the potential of 0.4 with a characteristic of a pseudoinductive behavior, being different from a capacitive and resistive curve presented at Pt/RGO catalysts. In this potential, Pt/PAA/RGO catalysts favor the formation of the adsorbed hydroxyl species, which is available to the removal of CO species. Thus, the size and dispersion of Pt nanoparticles on the surface of RGO control the electrocatalytic performance of Pt catalysts and the molecular pathway of methanol oxidation at the surface of Pt catalysts.

ACKNOWLEDGMENTS
The authors are most grateful to the National Natural Science Foundation of China (No.20903082).

References

1. H. J. Huang, D. P. Sun, X. Wang, *J. Phys. Chem. C* 115 (2011) 19405.

2. K. Scott, W. M. Taama, P. Argyropoulos, *J. Appl. Electrochem.* 28 (1998) 1389.
3. Y. H. Lin, X. L. Cui, C. H. Yen, C. M. Wai, *Langmuir* 21 (2005) 11474.
4. J. J. Wang, G. P.Yin, J. Zhang, Z. B. Wang, Y. Z. Gao, *Electrochim. Acta* 52 (2007) 7042.
5. X. L. Jin, B. He, J. G. Miao, J. H. Yuan, Q. X. Zhang, L. Niu, *Carbon* 50, (2012) 3083.
6. Y. L. Hsin, K. C. Hwang, C. T. Yeh, *J. Am. Chem. Soc.* 129 (2007) 9999.
7. Z. M. Cui, W. Xing, C. P. Liu, D. Tian, H. Zhang, *J. Power Sources* 195 (2010) 1619.
8. B. H. Wu, D. Hu, Y. J. Kuang, B. Liu, X. H. Zhang, J. H. Chen, *Angew. Chem. Int. Ed.* 48 (2009) 4751.
9. R. Ganesan, D. J. Ham, J. S. Lee, *Electrochem. Commun.* 9 (2007) 2576.
10. A. K. Geim, K. S. Novoselov, *Nat. Mater.* 6 (2007) 183.
11. S. J. Guo, S. J. Dong, E. K. Wang, *ACS Nan.* 4 (2010) 547.
12. W. Hummers, R. Offeman, *J. Am. Chem. Soc.* 80 (1958) 1339.
13. S. Park, J. H. An, I. W. Jung, R. D. Piner, S. J. An, X. S. Li, A. Velamakanni, R. S. Ruoff, *Nano Lett.* 9 (2009) 1593.
14. R. F. Nie, J. H. Wang, L. N. Wang, Y. Qin, P. Chen, Z. Y. Hou, *Carbon* 50 (2012) 586.
15. J. D. Qiu, G. C. Wang, R. P. Liang, X. H. Xia, H. W. Yu, *J. Phys. Chem. C* 115 (2011) 15639.
16. R. Sardar, J. W. Park, J. S. Shumaker-Parry, *Langmuir* 23 (2007) 11883
17. Q. X. Zhang, Q. Q. Ren, Y. Q. Miao, J. H. Yuan, K. K. Wang, F. H. Li, D. X. Han, L. Niu, *Talanta* 89(2012) 391.
18. J. Y. Hong, K. Y. Shin, O. S. Kwon, H. Kang, J. Jang, *Chem. Commun.* 47.(2011) 7182.
19. S. Park, D. A. Dikin, S. T. Nguyen, R. S. Ruoff, *J. Phys. Chem. C* 113 (2009) 15801.
20. N. I. Kovtyukhova, P. J. Ollivier, B. R. Martin, T. E. Mallouk, S. A. Chizhid, E. V. Buzaneva, A. D. Gorchinskiy, *Chem. Mater.* 11 (1999) 771.
21. D. Li, M. B. Müller, S. Gilje, R. B. Kaner, G. G. Wallace, *Nat. Nanotechnol.* 3 (2008) 101.
22. H. M. Tóháti, B. Botka, K. Németh, Á. Pekker, R. Hackl, K. Kamarás, *Phys. Status Solidi. B* 247 (2010) 2884.
23. J. Q. Liu, L. Tao, W. R. Yang, D. Li, C. Boyer, R. Wuhrer, F. Braet, T. P. Davis, *Langmuir* 26 (2010) 10068.
24. F. H. Li, F. Li, J. X. Song, J. F. Song, D. X. Han, L. Niu, *Electrochem. Commun.* 11 (2009) 351.
25. H. J. Park, J. Kim, J. Y. Chang, P. Theato, *Langmuir*, 24 (2008) 10467.
26. S. M. Choi, M. H. Seo, H. J. Kim, E. J. Lim, W. B. Kim, *Int. J. Hydrogen Energ.* 35 (2010) 6853.
27. S. Ghosh, C. R. Raj, *J. Phys. Chem. C* 114 (2010) 10843.
28. G. Markovich, C. P. Collier, J. R. Heath, *Phys. Rev. Lett.* 80 (1998) 3807.